International Journal of Heat and Mass Transfer 52 (2009) 210–221

Contents lists available at ScienceDirect

International Journal of Heat and Mass Transfer

journal homepage: www.elsevier.com/locate/ijhmt

Practical application of inverse heat conduction for wall condition estimation on a rotating cylinder

F. Volle, D. Maillet, M. Gradeck *, A. Kouachi, M. Lebouché

LEMTA, Nancy-University, CNRS, 2, Avenue de la Forêt de Haye – BP160, 54504 Vandoeuvre-lès-Nancy Cedex, France

ARTICLE INFO

Article history:
Received 22 December 2007
Received in revised form 12 April 2008
Available online 7 August 2008

Keywords:
Inverse solution
Heat conduction
Integral transforms
Impinging jet
Transient
Boiling convection

ABSTRACT

The solution of the linear, inverse, transient heat conduction problem (IHCP) in a cylindrical geometry is analysed. The rotating cylinder under investigation is experiencing boiling convection induced by the impingement of a water jet. The initial temperature is known, additional temperature measurements in time are taken with sensors positioned at a constant radius within the solid material, and the estimation of the wall heat flux at the external radius is sought. First, simulated temperature measurements inside the cylinder are processed in order to be used to estimate the wall heat flux. When noise is present in the data, some of the simulated results obtained using the least squares method exhibit oscillatory behavior, but these large oscillations are substantially reduced by the implementation of a regularization technique. Real experimental data are also used for the wall condition estimation and for the subsequent building of local boiling curves are plotted and discussed. The question of the possible effect of a temperature dependent conductivity on the reconstructed wall condition is also considered.

1. Introduction

Inverse problems are encountered in many heat transfer situations when severe working conditions make measurement of thermal properties or of unknown boundary conditions difficult. Inverse heat conduction techniques [1] can be implemented for estimating the heat flux values on the external surface of a conducting solid through the use of experimental temperature measurements taken within or at another surface of the body.

With the improvement of computer capability, inverse techniques have become a popular means of resolving heat transfer problems in the last decade. Important applications for inverse heat conduction problem solutions include for example controlled cooling of electronic components [2], estimation of jet-flow rate of cooling in machining [3,4] or quenching [5], and determination of conditions at the interface between the mold and metal during metal casting [6] or rolling process [7].

In boiling heat transfer research [8,9], inverse techniques are also very useful. In this type of situation, the temperature sensors cannot be placed directly on the surface due to the fact that the surface morphology has a direct influence on the phenomenon of interest. A method for measurement of local heat fluxes at the surface of a rotating cylinder which is experiencing boiling convection induced by the impact of a subcooled water jet on its surface has been recently proposed by Volle et al. [10]. It involves estimating the Neumann boundary condition on the outer surface of the cylinder starting from temperature measurements inside the cylinder. This two-dimensional inverse conduction method is based on an analytical solution of the energy equation and has been successfully tested on simulated temperature measurements. It can be used to study the influence on heat transfer of parameters such as water jet subcooling, nozzle-surface distance and surface velocity.

The purpose of this paper is not describing the boiling phenomena occurring when a subcooled jet impinges a hot surface. We want to test here the quality of the design of the corresponding experiment, where embarked thermocouples yield a temperature signal that has to be inverted using a pertinent heat transfer model in this heated rotating cylinder. This paper corresponds to the qualification of both the set-up, the model and the inversion procedure, where all causes of noise and biases have to be taken into account. Further implementation of this indirect measurement technique is currently under way, in order to characterize heat transfer in the different boiling regimes (especially film and transition boiling) on this type of moving surface. Corresponding literature values [11,12] for the case of a moving cylinder end this validation.

2. Direct heat transfer problem

The direct problem will be considered either as a one- or a two-dimensional problem (noted 1D and 2D, respectively), and in each case the linear (L) and non-linear (NL) approaches will be treated. Thus, for a better clarity and conciseness, the different cases that will be considered will be referred as C_x according to Table 1.

* Corresponding author. Tel.: +33 38 359 5559; fax: +33 38 359 5544.
E-mail address: michel.gradeck@ensem.inpl-nancy.fr (M. Gradeck).

0017-9310/$ - see front matter © 2008 Elsevier Ltd. All rights reserved.
doi:10.1016/j.ijheatmasstransfer.2008.05.025

Nomenclature

a	thermal diffusivity ($m^2\ s^{-1}$)
c	specific heat ($J\ kg^{-1}\ K^{-1}$)
h	heat transfer coefficient ($W\ m^{-2}\ K^{-1}$)
l	length of the cylinder (m)
N_{fts}	number of future time steps
N_H	number of harmonics
N_{TC}	number of thermocouples
p	Laplace parameter (s^{-1})
P	heating power (W)
r	radius (m)
t	time (s)
T_e, T^{SS}	ambient, initial temperature (°C)
$\boldsymbol{X_n}$	sensitivity matrix
$X_{i,k+1}$	sensitivity coefficients ($m^2\ K\ W^{-1}$)
$\boldsymbol{Y}$	vector of measured temperatures
Z_n	transfer function (m)

Greek symbols

γ	polar angle (rad)
λ	thermal conductivity ($W\ m^{-1}\ K^{-1}$)
ρ	density ($kg\ m^{-3}$)
σ	noise standard deviation (°C)
φ	heat flux ($W\ m^{-2}$)
ω	angular velocity ($rad\ s^{-1}$)

Subscripts

k	relative to the kth time interval Δt
m	relative to thermocouple m
n	relative to harmonic n

Superscripts

$-$	Laplace transform
$\sim$	Fourier transform
$\hat{}$	estimated value
t	transpose of a matrix

Table 1
Notations for considered cases

	L	NL
1D	C_{1L}	×
2D	C_{2L}	C_{2NL}

Moreover, when noise will be added to the generated data, the notation $C_{x\sigma}$ will be employed. If no noise is added, the case will be noted C_{x0}.

2.1. Two-dimensional linear modelling

In the direct problem, the exact temperature T at a point M inside a full rotating cylinder – composed of two layers of radii r_1 and r_2 – is sought as a function of polar coordinates (r,γ) as shown in Fig. 1. A uniform surface heat source dissipates a power P(W) at radius r_1 and a heat flux density φ_2, which varies with angle γ and with time t, is set at the outer radius r_2.

For each domain i (where subscript i designates temperature T in the central layer $(0 \leqslant r < r_1;\ i = 1)$ and in the outer layer $(r_1 < r \leqslant r_2;\ i = 2)$) of the rotating homogeneous cylinder, assuming constant thermophysical properties, the mathematical formulation of the two-dimensional heat conduction problem can be written in the laboratory coordinates system as

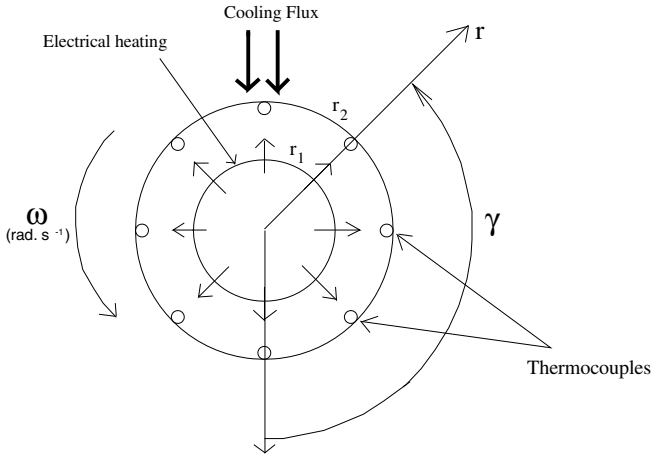

Fig. 1. Model geometry.

$$\frac{\partial^2 T_i}{\partial r^2} + \frac{1}{r}\frac{\partial T_i}{\partial r} + \frac{1}{r^2}\frac{\partial^2 T_i}{\partial \gamma^2} - \frac{\omega}{a}\frac{\partial T_i}{\partial \gamma} = \frac{1}{a}\frac{\partial T_i}{\partial t} \tag{1}$$

where a is the thermal diffusivity of the material and ω the angular velocity.

The associated boundary and interface conditions are

$$\begin{cases} T_i(r,\gamma+2\pi,t) = T_i(r,\gamma,t); \quad T_i(r,\gamma,t=0) = T^{SS}(r,\gamma) \\ \frac{\partial T_1}{\partial r}(r=0,\gamma,t) = 0; \quad -\lambda\frac{\partial T_2}{\partial r}(r=r_2,\gamma,t) = \varphi_2(\gamma,t) \\ T_1(r=r_1,\gamma,t) = T_2(r=r_1,\gamma,t) \\ \frac{P}{2\pi r_1 l} - \lambda\frac{\partial T_1}{\partial r}(r=r_1,\gamma,t) = -\lambda\frac{\partial T_2}{\partial r}(r=r_1,\gamma,t) \end{cases} \tag{2}$$

where T^{SS} is a steady-state temperature field that takes place in the cylinder before the cooling flux φ_2 is set.

The linear direct problem that is considered can then be solved by expressing temperature T in terms of function $\varphi_2(\gamma,t)$. The transient temperature $T^{transient}$ solution of system (1) and (2) can be written as the sum of the solutions of three problems:

$$T^{transient}(r,\gamma,t) = T^{relax}(r,t) + T^{adia}(r,t) + T^{cool}(r,\gamma,t) \tag{3}$$

In this equation, T^{relax} is the axisymmetrical 1D transient temperature field that results from the natural relaxation of the initial $T^{SS}(r)$ field inside the cylinder that is now insulated (adiabatic boundary at $r = r_2$) without internal heating ($P = 0$). T^{adia} is the axisymmetrical 1D transient temperature field produced by internal heating P at radius r_1 with an adiabatic boundary at $r = r_2$ and an initial zero temperature condition.

These problems can be independently solved [10] and we will consider here only the temperature field T^{cool} produced by the external cooling flux φ_2 that is solution of Eq. (1) associated to boundary conditions:

$$\begin{cases} T(r,\gamma+2\pi,t) = T(r,\gamma,t) \quad \text{(periodicity conditions)} \\ -\lambda\frac{\partial T}{\partial r}(r=r_2,\gamma,t) = \varphi_2(\gamma,t) \quad \frac{\partial T}{\partial r}(r=0,\gamma,t) = 0 \\ T(r,\gamma,t=0) = 0 \end{cases} \tag{4}$$

The semi-analytical solution, [10], utilizes Laplace (parameter p) and Fourier (harmonic number n) transforms, the temperature being given in the Fourier domain by

$$\widetilde{T}(r,n,t) = -\frac{1}{\lambda}\int_0^t [\widetilde{\varphi}_2(n,\tau)][e^{-j\ n\ \omega\ (t-\tau)} Z_n(t-\tau)]\,\mathrm{d}\tau, \tag{5}$$

with

$$\overline{Z}_n(r,p) = \frac{I_n\left(\sqrt{\frac{p}{a}}r\right)}{\sqrt{\frac{p}{a}} I'_n\left(\sqrt{\frac{p}{a}}\,r_2\right)} \tag{6}$$

A Fourier inversion of Eq. (5) allows the calculation of the original temperature $T(r,\gamma,t)$ in the initial domain at any point in the cylinder:

$$T^{\mathrm{cool}}(r,\gamma,t) = \frac{\widetilde{T}_0}{2\pi} + \frac{1}{\pi}\sum_{n=1}^{\infty}[\mathrm{Re}(\widetilde{T}_n)\cos(n\gamma) - \mathrm{Im}(\widetilde{T}_n)\sin(n\gamma)] \tag{7}$$

where Re and Im are, respectively, the real and the imaginary part of the Fourier transform.

In practice, this sum is truncated to a total number of harmonics N_H that depends on the space shape of the heat flux distribution φ_2. For the inversion phase, this N_H number is also limited by the measurement noise and by the number of discrete measurement points.

2.2. Direct simulation

Until now, no assumption has been made concerning the surface heat flux; it only has to vary with time t and with angle γ. Thus, the temperature field can be calculated with any heat flux imposed at radius $r = r_2$. However, the aim of the present study is to propose an inverse algorithm allowing to estimate heat fluxes extracted from the cylinder by the impact of a water jet: we consequently choose a heat flux function that is related to the phenomenon of interest, i.e., water jet cooling.

Thus, the analytical direct model is tested for a given heat flux imposed at radius $r = r_2$ in the fixed coordinates system that has a time exponential decay (characteristic time t_c) and a Gaussian shape in γ (simulating the decrease of cooling efficiency when moving away from the center of the jet)

$$\varphi_2(\gamma,t) = K_t \mathrm{e}^{-\frac{1}{2}\left(\frac{\gamma-\pi}{\sigma_c}\right)^2}\ \mathrm{e}^{-t/t_c} + \frac{P}{2\pi r_2 l} \tag{8}$$

The $\frac{P}{2\pi r_2 l}$ term in Eq. (8) allows to recover the steady-state asymptotic solution ($t \to \infty$). The characteristic time t_c allows to impose the cooling rate. For physical reasons, cooling rates will be higher for null or low values of angular velocity ω (hence a small value for t_c) than for large values of ω (high values of t_c).

Except where otherwise specified, the parameters used for the simulations are given in Table 2.

Temperature measurements are made through $N_{\mathrm{TC}} = 24$ thermocouples that are embedded in the moving cylinder at radius $r = r_{\mathrm{TC}}$. At time $t = 0$, when the jet impinges the cylinder, the thermocouple number i ($i = 1$ to N_{TC}) is at angle $\gamma_i(0)$. At a later time, its angle $\gamma_i(t)$ is given by

$$\gamma_i(t) = \gamma_i(0) + \omega t \tag{9}$$

The observed temperature for a thermocouple i, $T_i^{\mathrm{cool}}(t) = T^{\mathrm{cool}}(r_{\mathrm{TC}},\gamma_i(t),t)$, see Eq. (7), is calculated through a numerical quadrature (trapezoidal rule for Eq. (5)) with a $\Delta t = 0.1$ s time step for the plot.

Excitation $\varphi_2(\gamma_i(t),t)$, given by Eq. (8), as well as the temperature response obtained by the analytical solution (7) for a radius $r_{\mathrm{TC}} = r_2$, are plotted in Fig. 2 in the moving coordinates system related to the cylinder for a point located at angle $\gamma_i(0) = \pi$ at $t = 0$. The total number of harmonics used for the truncation of Eq. (7) is $N_H = 12$.

Table 2
Parameters used

Parameter	Value
λ	90.7 W m^{-1} K^{-1}
ρc	3 919 520 J m^{-3} K^{-1}
r_1, r_2, l	0.049 m, 0.0875 m, 0.2 m
P, K_t	6000 W, 10^6 W m^{-2}
ω, σ_c	6 rad s^{-1}, 0.465 rad

2.3. Effect of thermal-dependency of thermophysical properties

It can be noted that Nickel conductivity and volumetric heat vary significantly with temperature (about 25 percent between 50 °C and 600 °C for the conductivity).

Thus, as the analytical solution has been obtained for the linear case, the choice of taking average values for conductivity λ and ρc product should have a non-negligible impact on the solution.

The finite elements solver FlexPDE® allows the use of temperature dependent properties for calculation of the temperature field inside the cylinder. This field is solution of the non-linear version of the heat equation (Eq. (1))

$$\frac{1}{r}\frac{\partial}{\partial r}\left[\lambda(T) r \frac{\partial T_i}{\partial r}\right] + \frac{1}{r^2}\frac{\partial}{\partial \gamma}\left[\lambda(T)\frac{\partial T_i}{\partial \gamma}\right] - \rho c(T)\ \omega\ \frac{\partial T_i}{\partial \gamma} = \rho\ c(T)\ \frac{\partial T_i}{\partial t} \tag{10}$$

with its associated conditions (2). It is possible to plot in Fig. 3a the temperature variations obtained both for constant: $\overline{\lambda} = 53.55$ W/m K and $\overline{\rho c} = 4.7 \times 10^6$ J/m^{3}K, and temperature variable properties obtained by polynomial regression:

$$\begin{cases} \lambda(T) = 4.98\ 10^{-5}\ T^2 - 5.95\ 10^{-2}\ T + 65.17132 \\ \rho\ c(T) = -4.68\ 10^{-9}\ T^6 + 8.31\ 10^{-6}\ T^5 - 5.29\ 10^{-3}\ T^4 \\ \qquad\qquad +1.41\ T^3 - 1.38\ 10^2\ T^2 + 5.22\ 10^3\ T + 4.03\ 10^6 \end{cases} \tag{11}$$

When compared, we see that the two assumptions for thermophysical properties lead to the same qualitative results, with a gap between variations of temperatures increasing with time t (about 2 °C at time $t = 6$ s). Nevertheless, simulations of inversion shown further down demonstrate that the influence of this non-linear effect on the estimated flux is not very large because the use of a 1D model allows to compensate this error.

3. 1D linear reduced model

A reduced local analytical 1D model simulating the same direct problem (see Section 2) can be proposed with the aim of simplifying the inversion procedure.

Using the classical Laplace transformation of temperature T:

$$\overline{T}(r,p) = \int_0^{\infty} T(r,t)\ e^{-pt}\,\mathrm{d}t$$

and considering an initial temperature equal to 0 and a uniform flux $\varphi_2(t)$, the 1D analytical solution for temperature T is in the time domain

$$T(r,t) = -\frac{1}{\lambda}\int_0^t [\varphi_2(\tau)][Z_0(r,t-\tau)]\,\mathrm{d}\tau \tag{12}$$

with

$$\overline{Z}_0(r,p) = \frac{I_0\left(\sqrt{\frac{p}{a}}\,r\right)}{\sqrt{\frac{p}{a}}\, I_1\left(\sqrt{\frac{p}{a}}\,r_2\right)} \tag{13}$$

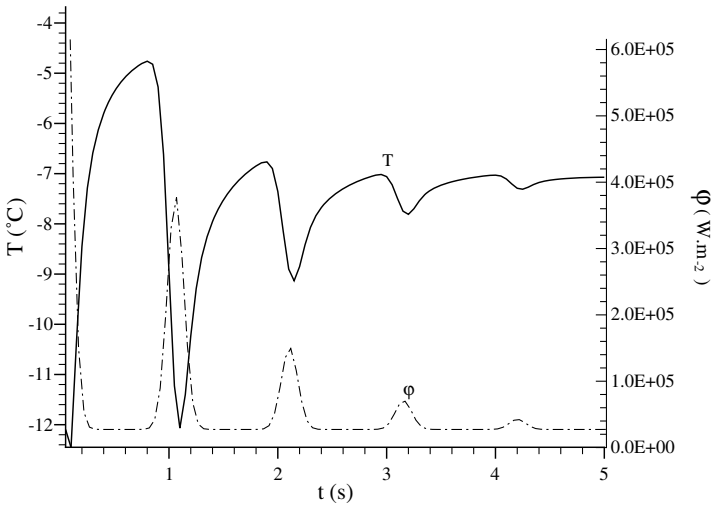

Fig. 2. Variations of $\varphi_2(t)$ and $T(t)$ for $r = r_2$, $\gamma(t=0) = \pi$ and $t_c = 1$ s.

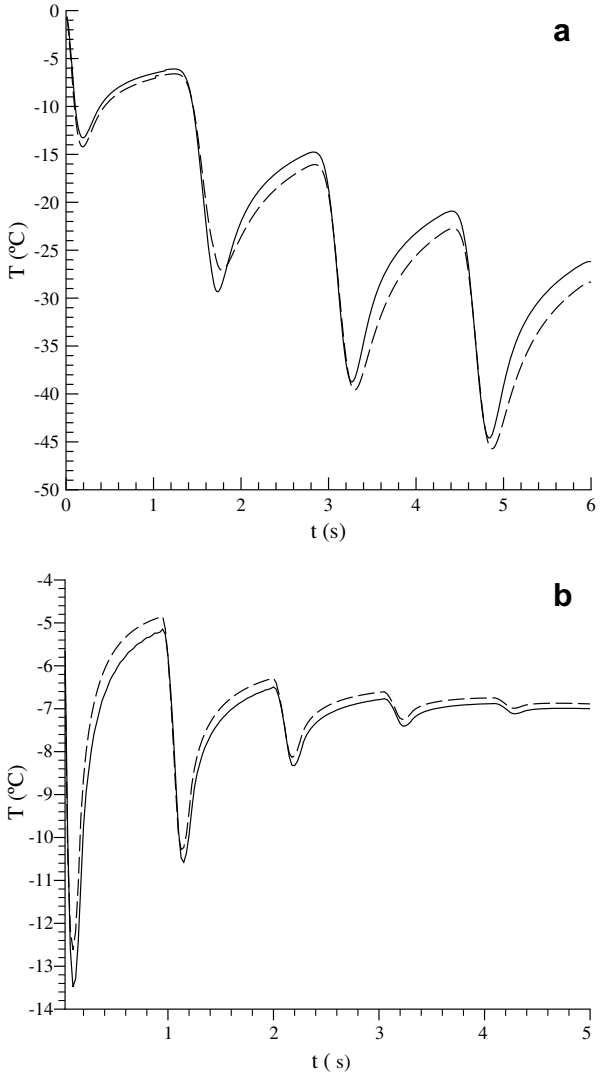

Fig. 3. Variations of $T(t)$ for two different cases. (a) Variations of $T(r = r_2, \gamma(t), t) - T^{SS}(r_2)$ for constant (——) and temperature dependent (– – –) properties, with $T^{SS}(r_2) = 550\,^{\circ}\mathrm{C}$, $\gamma(t=0) = \pi$ and $t_c = 1000$ s. (b) Variations of $T(t)$ using 2D (——) and 1D (– – –) model, for $r = r_2$, $\gamma(t=0) = \pi$ and $t_c = 0.5$ s.

This model consists in truncating Fourier inversion (8), taking only the $n = 0$ harmonics, assuming no γ dependency for the solution (wall heat flux density normal to the wall).

The temporal inversion of Eq. (13) is made using Stehfest's numerical algorithm [13,14]:

$$Z_0(r,t) = \frac{ln2}{t}\sum_{j=1}^{N} V_j\,\overline{Z}_0\left(r, p = \frac{j\ ln2}{t}\right) \text{ with } N = 10 \text{ in our case} \tag{14}$$

Moreover, since $Z_0(r, t-\tau) \to \infty$ when $t \to \tau$, an asymptotic behavior $\breve{Z}_0(r, t-\tau)$ is used for $Z_0(r, t-\tau)$ for time values lower than $t_{\lim} = i_{\lim}\Delta t$ ($i_{\lim} = 1$ in our case), hence

$$T(r,t) = -\frac{1}{\lambda}\left[\int_0^{t-t_{\lim}} \varphi_2(\tau)\ Z_0(r, t-\tau)\,\mathrm{d}\tau + \int_{t-t_{\lim}}^{t} \varphi_2(\tau)\ \breve{Z}_0(r, t-\tau)\,\mathrm{d}\tau\right] \tag{15}$$

with

$$\breve{Z}_0(r,t) = \sqrt{\frac{a}{\pi\ t}\frac{r_2}{r}}\ e^{-\frac{(r_2-r)^2}{4at}} + \frac{1}{2}\frac{a}{\sqrt{r\ r_2}}\ \mathrm{erfc}\left[\frac{r_2 - r}{2\ \sqrt{a\ t}}\right] \tag{16}$$

The 1D temperature response $T(r,t) = T(r, \gamma(t), t)$ (given by Eq. (12)) to the excitation $\varphi_2(t) = \varphi_2(\gamma(t), t)$ (given by Eq. (8)) is plotted in Fig. 3b for a point located at angle $\gamma(t)$ with $\gamma = \pi$ at time $t = 0$.

In this local use of Eq. (12), φ_2 is the flux variation at the same angle as the rotating point whose temperature is calculated.

In Fig. 3b, the temperature response calculated with the 2D analytical model (Eq. (7)) is also plotted. We see that the two models are nearly equivalent. Use of a linear 1D model produces a bias in the temperature output when compared to the corresponding output of a more detailed linear 2D model (and hence a bias in the estimated wall heat flux when the temperature measurements are inverted using this simpler model). However, a bias also exists when the output of the linear 2D model is compared to the response of a non-linear (thermophysical properties of the cylinder material depending on temperature) 2D model. We show here that there is a bias compensation when both effects are taken into account: for the very specific material we use (Nickel), the output of the linear 1D model is closer to the output of the non-linear 2D model than the output of the linear 2D model. This positive effect justifies the use of the linear 1D model (whose inversion is significantly less time consuming) for inverting the measurements.

4. Inverse problem

In the inverse problem, the condition relative to flux φ_2 (which is now unknown) is replaced by a measured temperature condition, the transient measurements being made by $N_{TC} = 24$ temperature sensors located at radii $r = r_{TC}$. All other quantities appearing in the formulation of the physical problem (thermophysical properties, ...) are assumed to be exactly known, but the measurements may contain random errors.

4.1. Inversion algorithm

In practice, the problem is solved in the particular case where $\varphi_2(\gamma, t)$ is a piecewise constant function of time t:

$$\varphi_2(\gamma, t) = \varphi_{2,k}(\gamma) \text{ for } t_k \leqslant t \leqslant t_{k+1} \tag{17}$$

with $t_k = k\Delta t$ and $k \geqslant 0$, where Δt is both a discretization time step for φ_2 and a calculation time step for temperature T.

It yields for $t_i = i\ \Delta t$ ($i \geqslant 2$) and with $t_0 = 0$:

$$T(r,\gamma,t_i) = -\frac{1}{\lambda}\left[\sum_{k=0}^{i-2}\varphi_{2,k}\int_{t_k}^{t_{k+1}} Z_0(r,t_i-\tau)\,\mathrm{d}\tau + \varphi_{2,(i-1)}\int_{t_i-t_{\lim}}^{t_i}\breve{Z}_0(r,t_i-\tau)\,\mathrm{d}\tau\right] \tag{18}$$

Temperature $T(r,\gamma,t_i)$ is thus a linear combination of the $\varphi_{2,k}$'s:

$$T(r,\gamma,t_i) = \sum_{k=0}^{i-1} X_{i,k+1}\ \varphi_{2,k} \tag{19}$$

where the coefficients $X_{i,k+1}$ are:

$$X_{i,k+1} = -\frac{1}{\lambda}\int_{t_k}^{t_{k+1}} L^{-1}\left[\frac{I_0\left(\sqrt{\frac{p}{a}}\,r\right)}{\sqrt{\frac{p}{a}}\,I_1\left(\sqrt{\frac{p}{a}}\,r_2\right)}\right]_{t_i-\tau}\mathrm{d}\tau \quad \text{if } k < i - i_{\lim} \tag{20}$$

and

$$X_{i,k+1} = -\frac{1}{\lambda}\int_{t_k}^{t_{k+1}}\breve{Z}_0(r,t_i-\tau)\,\mathrm{d}\tau \text{ if } k \geqslant i - i_{\lim} \tag{21}$$

This yields in a matrix form

$$\mathbf{T} = \begin{pmatrix} T(r,t_1)\\ \vdots \\ T(r,t_i)\end{pmatrix} = \begin{pmatrix} X_{11} & \dots & 0\\ \vdots & \ddots & \vdots \\ X_{i1} & \dots & X_{ii}\end{pmatrix}\begin{pmatrix}\varphi_{2,0}\\ \vdots \\ \varphi_{2,i-1}\end{pmatrix} = X\ \varphi_2 \tag{22}$$

where matrix X is the *sensitivity matrix*, which defines the relationship between a change in the surface heat flux and the corresponding change in the computed temperature response.

If $T(r_{TC}, \gamma_m(t), t)$ is the vector of exact temperatures measured by the mth thermocouple, Eq. (22) can be solved to find vector φ_2. Actually, experimental measurements always present some uncertainty, and the above method is no longer valid. We call $Y(r_{TC}, \gamma_m(t), t)$ the value of $T(t)$ measured at radius r_{TC} and angle $\gamma_m(t)$. Assuming an additive random error, we have

$$Y_m(t_i, \varphi_2) = T_m(t_i, \varphi_2) + \epsilon_{mi} \tag{23}$$

where ϵ_{mi} ($m = 1$ to N_{TC}, $i = 1$ to i_f) is an uncorrelated, zero mean and identically distributed normal noise of constant standard deviation σ.

To take this noise into account, it is possible to use an Ordinary Least Squares (OLS) method [15] which consists in minimizing the sum S of the square errors between computed and measured values

$$S_m = (Y_m - X\ \varphi_2)^t (Y_m - X\ \varphi_2) \tag{24}$$

with respect to the unknown heat flux vector φ_2. Solving for vector φ_2 gives

$$\hat{\varphi}_2 = (X^t X)^{-1}\ X^t\ Y_m \tag{25}$$

However, the inverse problem can be inherently ill-posed, which means that experimental errors may have a strong impact on the solution. Indeed, this ill-posedness results in high sensitivity to data errors due to the poor conditioning of the $\boldsymbol{X^t X}$ matrix. In this case, a regularization consisting in modifying least-square problem (24) will be required.

4.2. Regularization technique

In our case, the temporal regularization is afforded by Beck's future time steps method [1]. This method consists in seeking only a single heat flux component $\varphi_{2,M-1}$, corresponding not only to the "current" temperature measurement time $t = M\Delta t$, but also to the measured data from several future times steps N_{fts}. With the extra data, the problem is overdetermined and no additional unknowns are introduced: Beck's prescription is then to choose the unknown value of the heat flux component $\varphi_{2,M-1}$ so that the sum of the squares of the errors is minimized. Thus, at each time step t_M, a single value of heat flux is estimated considering the N_{fts} future times data points. However, the method requires to know the heat flux variations on the N_{fts} future times, and usually the temporary (and biased) assumption that $\varphi_{M-1} = \varphi_M = \cdots = \varphi_{M+N_{fts}-1}$ has to be made. After the flux component φ_{M-1} is estimated, the time index is advanced to t_{M+1} and the next component φ_M is estimated the same way.

Regularization in this sequential function specification method is afforded by the number of future times N_{fts} considered. Of course, this regularization introduces a bias, as the assumption $\varphi_{M-1} = \varphi_M = \cdots = \varphi_{M+N_{fts}-1}$ is made, and in fact the heat flux function is biased toward a constant value: a good compromise has to be made between stability and precision in the estimation.

Thus, a point of very practical importance is the selection of proper value for the regularization parameter N_{fts}: its level must be adjusted as a function of the noise in the data. In this work, we have chosen to minimize the following norm based on the estimated and exact heat flux densities:

$$e_{\varphi_2} = \sqrt{\frac{1}{N}\sum_{i=1}^{n}(\varphi_2 - \hat{\varphi}_2)^2} \tag{26}$$

Another approach would have been to invoke the "discrepancy principle", whose idea is to select N_{fts} as small as possible and such that the temperature residual

$$R_T = \sqrt{\frac{1}{N}\sum_{i=1}^{n}(Y - X\hat{\varphi}_2)^2} \tag{27}$$

is consistent with the measurement error in the data, which means of the same order of magnitude. This recommendation, made by Tikhonov et Arsenine [16], will be verified during our simulations.

4.3. Inversions from simulated measurements

In order to test the inverse algorithm, we implement it on simulated measurements. These simulated measurements (or synthetic data) come from the temperature distribution $T(r, \gamma(t), t)$, the output of the direct model (see Eq. (7)), which is modified by a random Gaussian additive noise ϵ, of standard deviation σ, according to Eq. (23). The output $\hat{\varphi}_2$ of the analytical inverse algorithm is an estimate of the heat flux φ_2, the input of the direct model. It should be noted that only a linear one-dimensional

(noted C'_{1L}) has been considered. Thus, in our simulations, the case noted $C_{2NL\sigma}/C'_{1L}$ will mean that the synthetic data have been obtained using a 2D non-linear direct solution perturbated by a noise of standard deviation σ, and that the inversion has been made using a 1D linear inverse algorithm. A flowchart of the inversion algorithm is proposed (in Fig. 4).

4.3.1. Case of a noiseless signal ($\sigma = 0$)

Here, the idea is to quantify the impact of the 1D linear approximation (15) on the inversion. To do so, the analytical 1D inverse algorithm is applied on the 2D linear temperature response (7) to the Gaussian excitation (given by Eq. (8)) (case C_{2L0}/C'_{1L} with our notations). The result is presented in Fig. 5, with a time step $\Delta t = 10^{-2}$ s.

A good agreement appears between the two curves, the mean square error being only a few percent. This can be explained by the fact that the rotation of the cylinder has a tendency to make temperature uniform in the angular direction. This temperature field is sketched in Figs. 6 and 7 inside the rotating cylinder at time $t = 5$ s, for the excitation of the cylinder by the Gaussian heat flux for different values of angular velocity ω and radius r. We can see that in the case of a static cylinder (Fig. 6), heat transfer is mainly two-dimensional as a temperature difference builds up between points located at different angular positions; this effect is less apparent for deeper radii. On the contrary, the inner temperature distributions flatten for non-zero angular velocity (Fig. 7), which means that the faster the cylinder is rotating, the more localized in a thin layer at the periphery of the cylinder heat transfer is: the one-dimensional assumption becomes more justified in this rotating case.

4.3.2. Case of a noise with a standard deviation $\sigma \neq 0$

When applied to noised temperatures, we see in Fig. 8 that the inverse method seems to be reliable for agreement between $\hat{\varphi}_2$ and φ_2 is quite good (case $C_{2L\,\sigma}/C'_{1L}$). In the absence of regularization ($N_{\text{fts}} = 0$), a noise of standard deviation $\sigma = 0.5$ °C leads to important oscillations of $\hat{\varphi}_2$. In the case of non-zero values for N_{fts} (5 and 15), for the same noise level, the inverse model yields the general shape of the direct flux φ_2, agreement between $\hat{\varphi}_2$ and φ_2 becoming quite good in the first case. Indeed, if the value of N_{fts} is too high (e.g. $N_{\text{fts}} = 15$), the effect of the determinist bias (introduced by the assumption $\varphi_{M-1} = \varphi_M = \cdots = \varphi_{M+N_{\text{fts}}-1}$) becomes apparent. The estimated heat flux variations are quenched

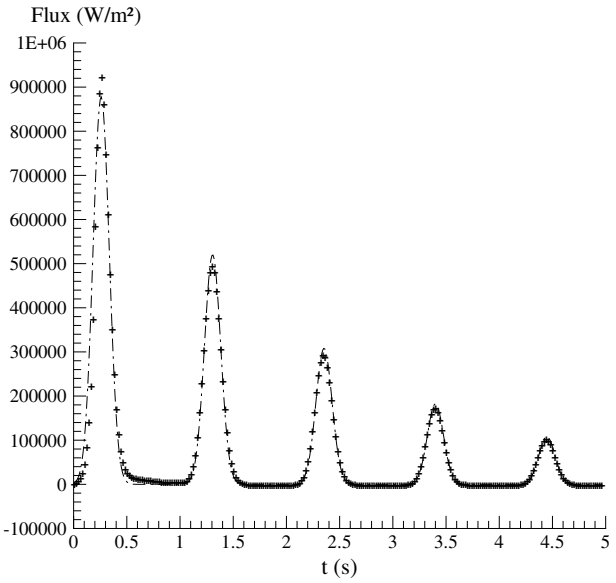

Fig. 5. Estimation using a 1D model: comparison between exact (–·–·–) and estimated (+) fluxes, with $t_c = 2$ s.

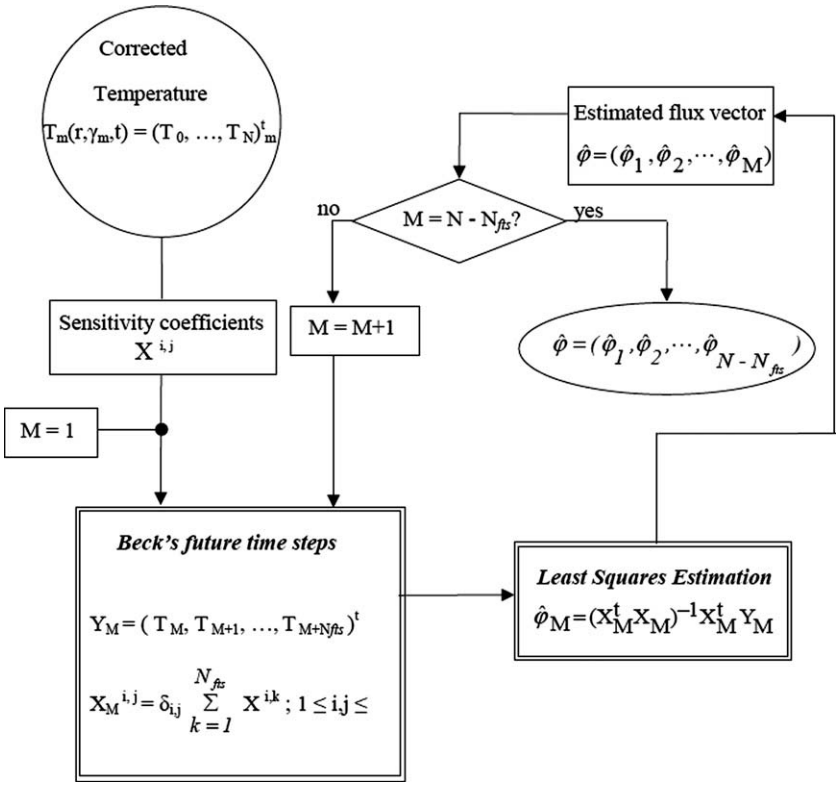

Fig. 4. Inversion algorithm.

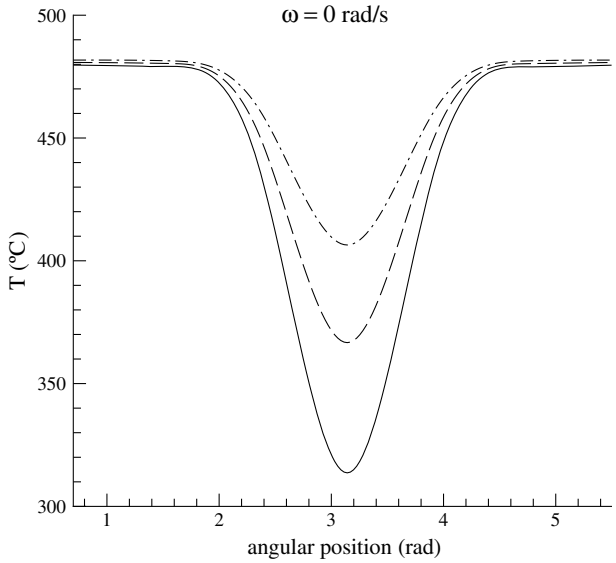

Fig. 6. Inner temperature distributions at time $t = 5$ s for $\omega = 0$ rad/s and for $r = 0.0871$ m (———), $r = 0.0831$ m (– – – –) and $r = 0.0791$ m (–·–·–).

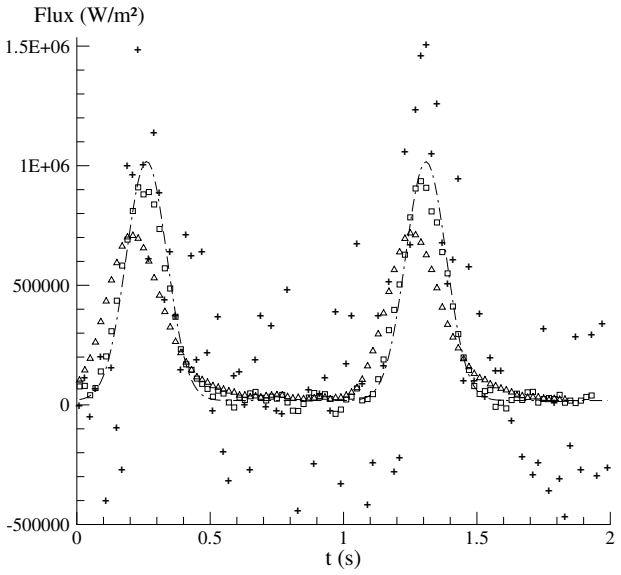

Fig. 8. Influence of parameter N_{fts} on the estimation with $\sigma = 0.5$ °C and $t_c = 1000$ s (——, exact flux; +, $N_{fts} = 0$; □, $N_{fts} = 5$; △, $N_{fts} = 15$).

and the rise in the heat flux occurs earlier in time, owing to the anticipation of the temperature response associated with the use of future time information (see Fig. 9).

Other simulations have shown that neglecting the two-dimensional effects tends, as one could expect it, to overestimate the heat flux, especially in the static case ($\omega = 0$).

4.4. Estimation error

Any inverse algorithm can produce an estimate of the desired function. It is then of primary importance to quantify the estimation error in order to quantify the accuracy of the inversion. In our case, the error can be divided into several components:

- –the error linked to measurements errors (whose influence can be decreased thanks to regularization);
- –the error due to the different quadratures used for calculation of Laplace transforms ($\sum$ instead of $\int$), error that is negligible when the integration time step Δt becomes small enough;
- –the error due to the uncertainties on the parameters supposed to be known: temperature sensors positions and thermophysical properties.

4.4.1. Sensitivity to temperature error and choice of parameter N_{fts}

As explained before, a point of very practical importance is the selection of proper value for the regularization parameter N_{fts}. To assess this value, variations of norms e_{φ_2} and R_T with parameter N_{fts} are plotted in Fig. 10 for a noise ϵ having a standard deviation $\sigma = 0.5$ °C, and an inversion time step $\Delta t = 10^{-2}$ s.

We see that the adjusted value of N_{fts} that minimized e_{φ_2} is $N_{fts} = 4$. It should be noted that for this value of N_{fts}, the temperature residual R_T is very close to the measurement error, as recommended by Tikhonov et Arsenine [16].

Lastly, simulated measurements without any noise were used as an input of the inverse algorithm for this adjusted value of parameter N_{fts}. The estimated heat flux $\hat{\varphi}_2$ was very close to the

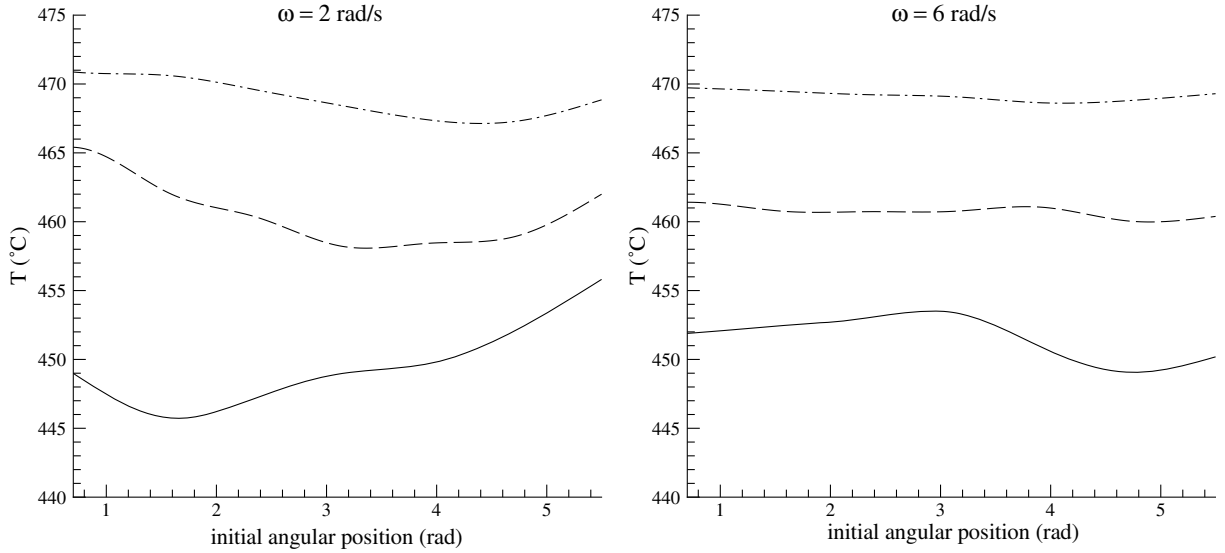

Fig. 7. Inner temperature profiles at time $t = 5$ s for $\omega = 2$ rad/s (left) and $\omega = 6$ rad/s (right), for $r = 0.0871$ m (———), $r = 0.0831$ m (– – – –) and $r = 0.0791$ m (–·–·–).

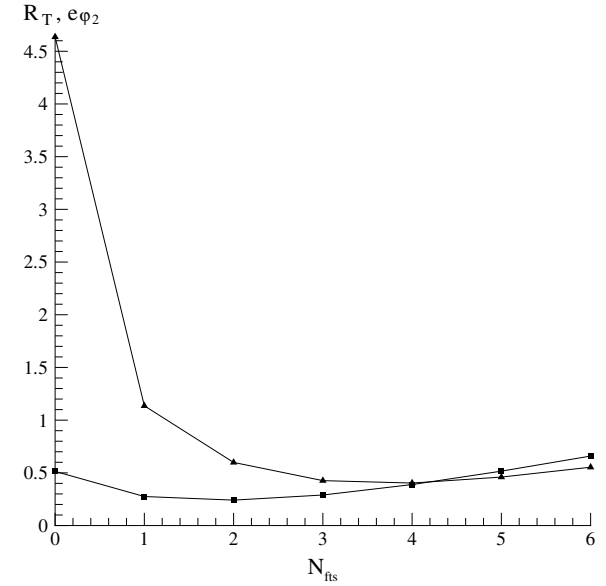

Fig. 9. Variations of mean residual R_T (■) and mean square error e_{φ_2} (▲).

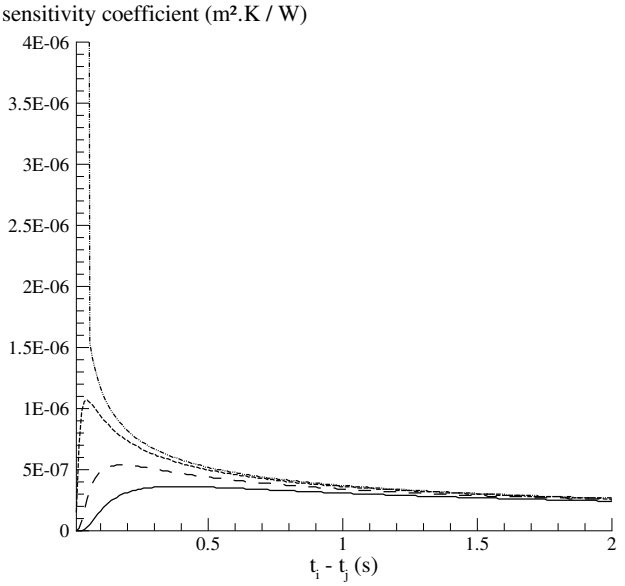

Fig. 10. Influence of the measurement depth on the sensitivity coefficients (–·–·–·–, depth = 1 mm; – – – –, depth = 2 mm; — — —, depth = 3 mm; ——-, depth = 4 mm).

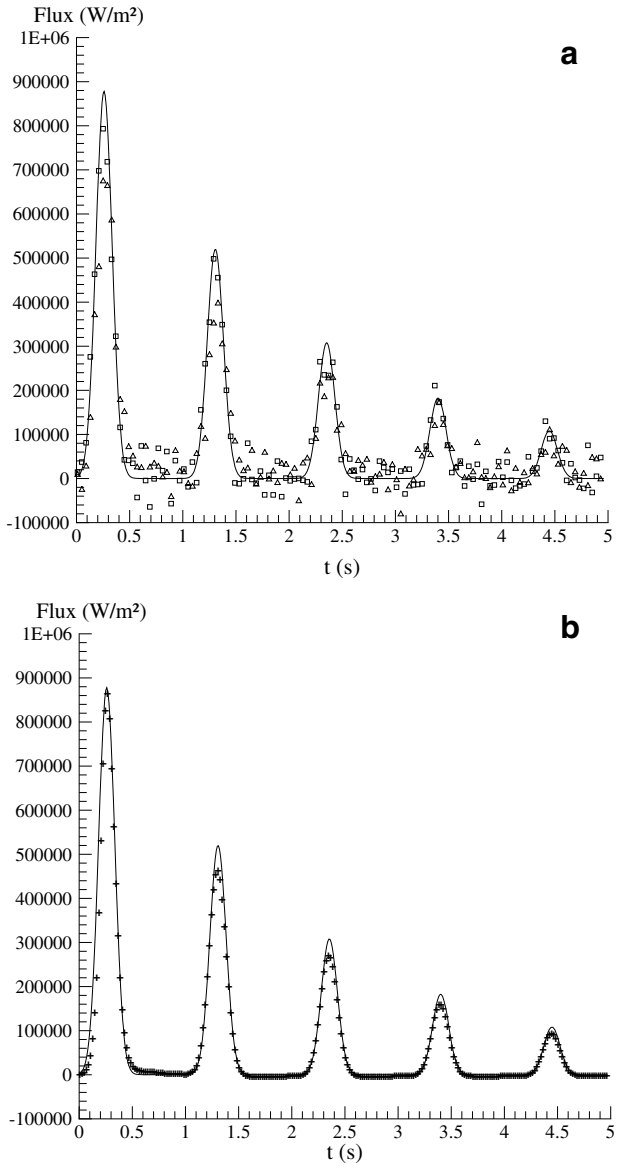

Fig. 11. Influence on the estimation of known parameters. (a) Influence on the estimation of an error on the measurement radius, with $\sigma = 0.5$ °C (——, exact flux; □, $r_{TC} = r_{nominal}$; △, $r_{TC} < r_{nominal}$). (b) Influence on the estimation of the constant thermophysical properties assumption: comparison between exact (— — —) and estimated (+) heat fluxes.

original one, which shows that the determinist bias (introduced by the regularization) is very small.

4.4.2. Error on the probes' locations

In practice, as temperature measurements are made inside the body under investigation, it is useful to study the sensitivity coefficient X_{ij} of temperature T_i (at time t_i) to the surface heat flux densities φ_j ($j \leqslant i$). This coefficient, defined as

$$X_{ij} = \frac{\partial T_i}{\partial \varphi_j} \tag{28}$$

does not depend on the heat flux boundary condition due to the linearity of the problem. It only depends on the temporal difference $t_i - t_j$ (a characteristic of convolution problems). As shown in Fig. 11, where X_{ij} is plotted for different values of the measurement depth, the radial position has an influence on the sensitivity of temperature to the surface heat flux: the deepest the measurement is made, the less the sensitivity and the more difficult the estimation is. This influence is amplified when noised temperatures are used. As a consequence, in this part we will study the error due to the uncertainties on the temperature sensors locations by taking into account the temperature noise. We will consider the worst case corresponding to a thermocouple located deeper in the cylinder than it is supposed to be ($r_{TC} < r_{nominal}$).

The inversion procedure is as follow:

- The temperatures "seen" by a thermocouple located at angle $\gamma = \frac{\pi}{2}$ at time $t = 0$ are calculated for radii $r_{TC} = r_{nominal}$ and $r_{TC} = 99.54\%\ r_{nominal}$, which corresponds to depths of 0.4 and of 0.8 mm, respectively.
- The calculated temperature fields are noised by an additive noise of standard deviation $\sigma = 0.5$ °C.

- These "experimental" data are used for the inversion using a unique radius equal to $r_{nominal}$ (i.e. 0.4 mm).
- By comparing the estimated and exact fluxes (see Fig. 11a) and calculating the mean square errors, it is possible to quantify the estimation error linked to the uncertainties on the probes' locations. This simulation corresponds to case $C_{1L\sigma}/C'_{1L}$.

It is interesting to notice in Fig. 11a that the two assumptions for the measurement radius lead to nearly the same profile, even if the heat flux is underestimated when the measurement radius r_{TC} is lower than the nominal radius $r_{nominal}$ because temperature gradients are damped (typical of heat conduction). Besides, the mean square error e_{φ_2} is 0.31×10^5 W m^{-2} when measurement is made at $r_{TC} = r_{nominal}$ (which corresponds to a depth of 0.4 mm), and 0.57×10^5 W m^{-2} when $r_{TC} < r_{nominal}$ (depth of 0.8 mm).

4.4.3. Error due to the constant thermophysical properties assumption

As explained before, the problem has been analytically solved considering constant thermophysical properties. It appeared in Section 2.3 that this assumption had an influence on the calculated temperatures, influence that should also appear during the estimation process.

In order to quantify this influence, we applied the 1D linear inverse algorithm on synthetic temperatures calculated by the FlexPDE® solver using temperature dependent properties (case C_{2NL0}/C'_{1L}). The comparison between direct and estimated heat fluxes is shown in Fig. 11b.

We see a good agreement between the two curves, the mean square errors e_{φ_2} being about 0.3×10^5 W/m^2: thus, the error due to the use of a 1D linear inverse algorithm (applied to the response of a 2D non-linear direct model) is of 6% only.

5. Examples of an experimental inversion

The experimental validation of the inversion method has been done on a set of experiments [17,18]. Thus, a complete description of the experimental set-up can be found in the previous papers.

5.1. Experimental set-up

The main characteristics of the set-up used for the experiments [11,12] are given here. A rotating cylindrical of 200 mm length, 49 mm inside radius and 87.5 mm outside radius is instrumented with 24 thermocouples of 0.5 mm diameter, used to measure local transient temperature near the surface. They are embedded parallel to the cylinder axis. Their junctions are located in the transverse plane of symmetry of the cylinder. The nominal radius of implantation is $r_{TC} = 86.5$ mm.

A uniform and time-constant surface heat source P(W) is dissipated through three electrical wires inserted into grooves machined in the internal surface of the external cylinder, in order to reach the desired initial surface temperature.

The measurement cylinder, see Fig. 12, is submitted to the impingement of a subcooled water jet whose temperature and velocity were known. The nozzle/surface distance was also known, and it consisted in another parameter which could influence the cooling rates.

5.2. Experimental procedure

The experimental procedure is as follow: when the surface temperature had reached the desired value, the heating of the cylinder is stopped and the jet cooling starts simultaneously while the transient temperatures were measured by the thermocouples. Measurements are made for different jet velocities, jet temperatures, initial surface temperatures and for different cylinder's angular velocities.

The temperature measurements are used as the input of the 1D inverse algorithm in order to estimate the heat flux extracted by the impact of the subcooled water jet. In fact, since in our inverse conduction problem we are only interested in the estimation of the wall heat flux, we have inverted the cooling component $T = T^{cool}$ only. Thus, in our experiments, $T^{SS}(r)$ was measured by the rotating thermocouples prior to jet impingement, which allowed to calculate $T^{relax}(r,t)$ with $T^{adia}(r,t) = 0$ (no heating during jet cooling) at the same locations to get the experimental T^{cool} response by

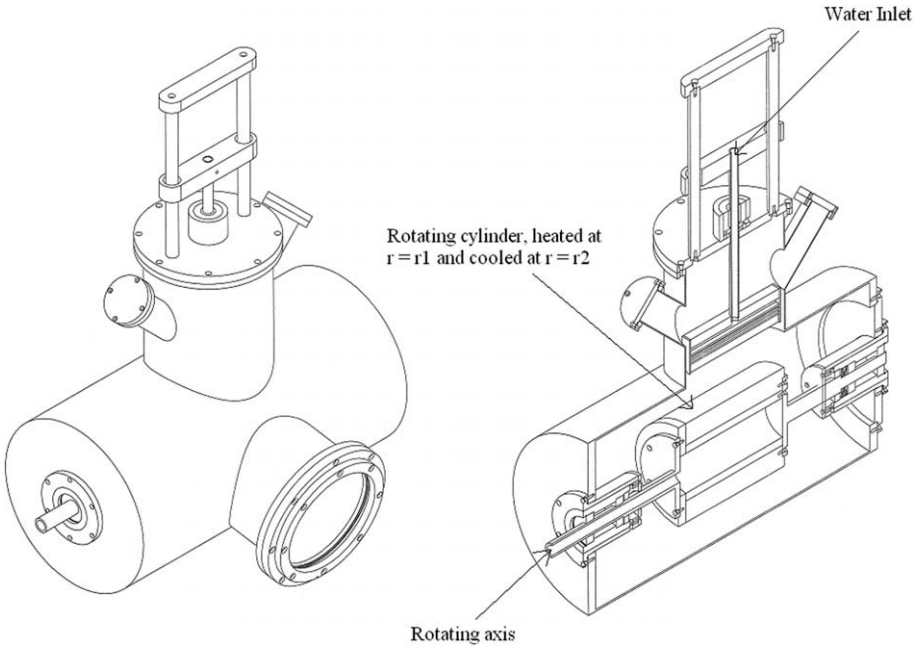

Fig. 12. Experimental set-up from [11,12].

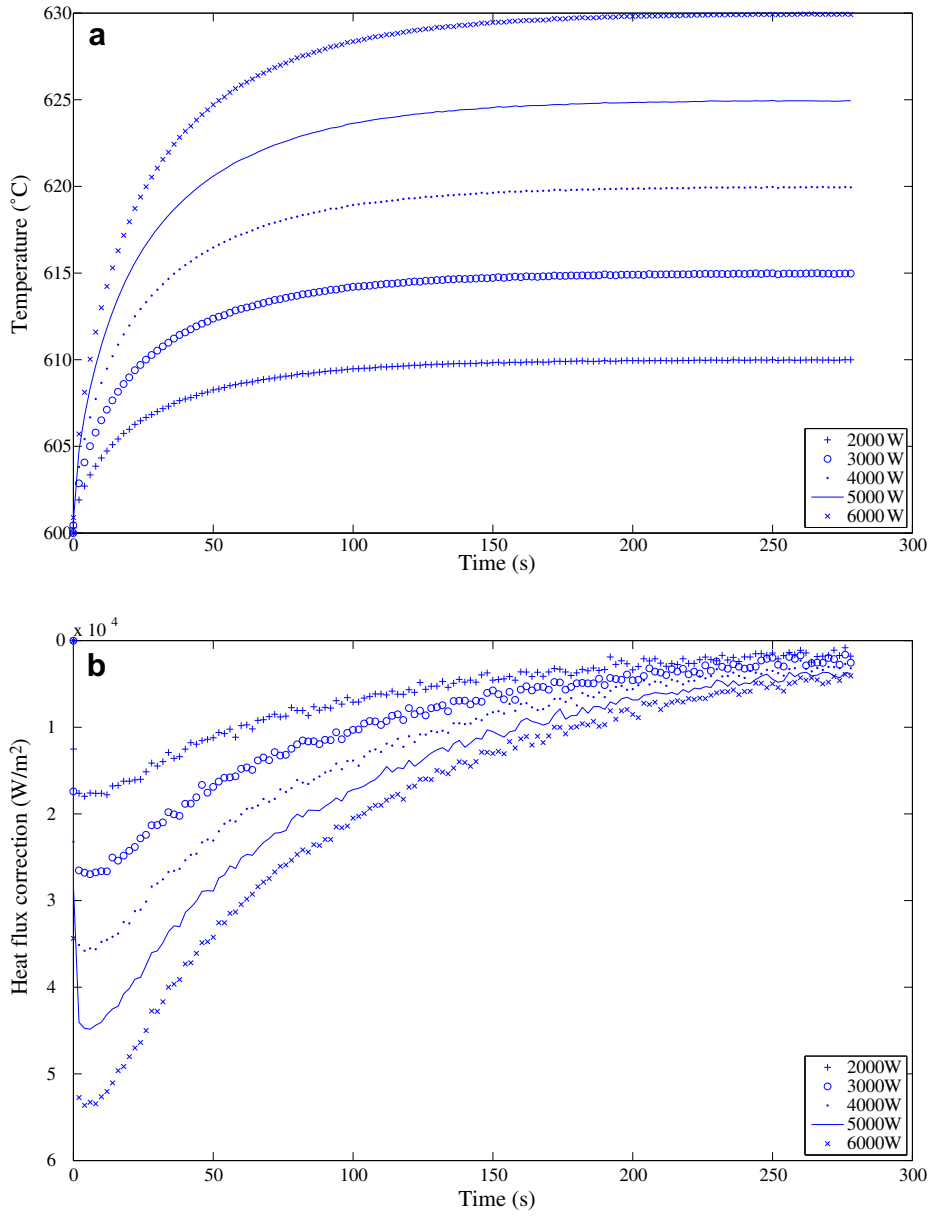

Fig. 13. Relaxation temperature and corresponding heat flux correction for different internal heating power. (a) Corrected temperature, (b) heat flux correction.

substraction from the experimental signal. As the problem is linear, the correction due to the natural relaxation of the temperature $T^{relax}(r,t)$ when the internal heating has been stopped (i.e. before the jet cooling) can be calculated independently of each experiment. The heat flux correction will depend only on the internal heating power but these are independent of the initial external wall temperature. Fig. 13 shows the heat flux corrections for different internal heating power. These flux corrections are negative and produce hence an increase of the cooling flux. It shows that the correction is quite high at the very beginning of the experiment and becomes negligible for longer times.

In a later step, once the heat flux estimated, the wall temperature can be reconstructed by application of the direct problem (3) and (14) in order to plot boiling curves for example.

The advantage of the method lies in the fact that it is non-intrusive which allows to quantify the effect of different parameters on the cooling rates and on the boiling phenomena that can occur at the surface of the cylinder.

5.3. Experimental inversion results for a rotating cylinder case

Fig. 14 shows the experimental temperature measured during impingement of the rotating cylinder ($\omega = 15$ rad/s) by a water jet of temperature $T_j = 66\,^{\circ}$C and jet velocity $V_j = 1.06$ m/s, for heating power $P = 2000$ W. The surface velocity is equal to $V_S = 1.32$ m/s and thus the surface to jet velocity ratio r^* is 1.25 with a 50 mm nozzle to cylinder distance. A zoom between times $t = 225$ s and $t = 230$ s shows that the observed oscillations are due to the rotation of the cylinder, the curve being composed of an increasing and a decreasing phase. The decreasing phase corresponds to jet cooling and the increasing phase to re-heating of the surface when the thermocouple has left the zone of influence of the jet. Fig. 15 shows the resulting absolute values of the estimated wall heat flux variations with time.

The zones of existence of different boiling regimes are indicated in these figures: (1) film boiling, (2) transition boiling, (3) nucleate

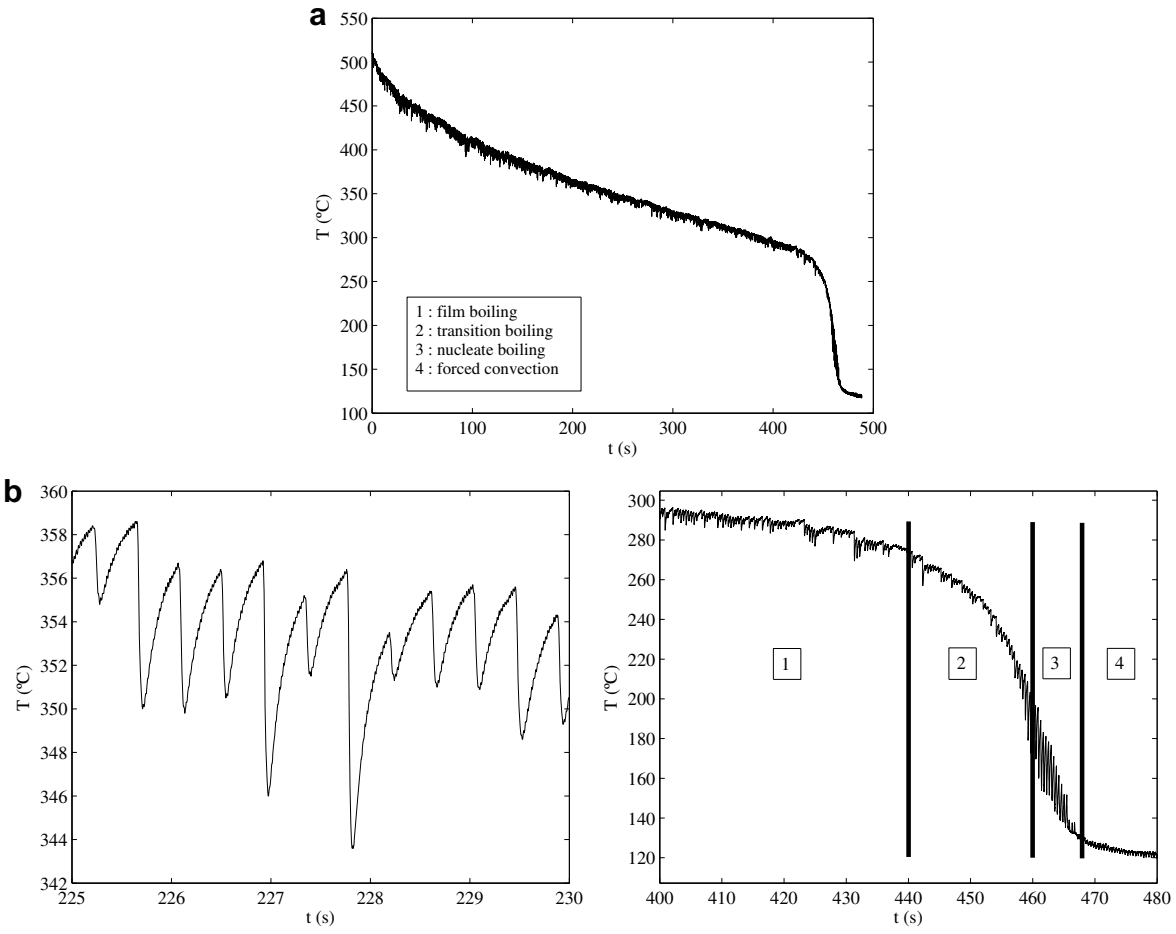

Fig. 14. Experimental temperature in rotating case. (a) Experimental temperature, (b) experimental temperature in film boiling and end of cooling.

boiling and (4) forced convection. The limits between zones can be determined by plotting the estimated boiling curves ($\widehat{\varphi}_2$ versus ΔT_{sat}) in the laboratory coordinates system: minimum heat flux for film/transition, maximum heat flux for transition/nucleate, and angular point for nucleate/forced convection.

The maximum heat flux – corresponding to the critical heat flux – is of the order of 3.5 MW/m^2 (see Fig. 15).

6. Conclusion

A two-dimensional linear analytical solution has been used for calculation of the transient temperature response of a finite-length rotating heated cylinder submitted to a known but time-dependent and not uniform cooling heat flux at its outer surface. This solution, based on Laplace and Fourier transforms, is obtained by solving the heat equation and is explicitly given using series expansions and modified Bessel functions. The variations of thermophysical properties of Nickel with temperature have been taken into account. It has been shown that the linear model can be used for transient simulations with low error. A further simplification of the model, that consists in making it locally 1D, has been achieved and justified.

Then, simulations with or without additive noise have shown that an estimation technique with time regularization applied to experimental temperatures allows to recover the surface heat flux with good accuracy. Some kind of time regularization, here Beck's future time steps methods, is compulsory because temperature measurements are made inside the body rather than at the boundary (hence a great sensitivity to measurement errors). The limitation of the method (and of any inversion method) is the usual trade-off that has to be made between a stable solution starting from noised measurements and the estimation bias (caused by a too large regularization). Other causes of estimation bias have been studied: error in the precise location of the sensors, temperature dependency of thermophysical properties, and inversion by a reduced linear 1D model.

The interest of using a 1D analytical method lies in the minimum number of hyperparameters that are used (one here: the number of future times N_{fts}): no space grid nor meshing is necessary, with its associated effect on the error in the estimated flux. Moreover, the time needed for calculation is quantitatively reduced when the analytical approach is used. A specific limitation of the analytical method is the necessity to have non-temperature dependent thermophysical properties of the cylinder (linear estimation problem), but the influence of this assumption on the inversions can be quantified.

This indirect method of measurement allows to consider the rotative cylinder as a non-intrusive fluxmeter: it has allowed to plot local boiling curves, including the transition boiling regime, without perturbing the phenomena of interest. The detailed use of this technique for boiling characterization on a moving cylinder is studied in [17,18].

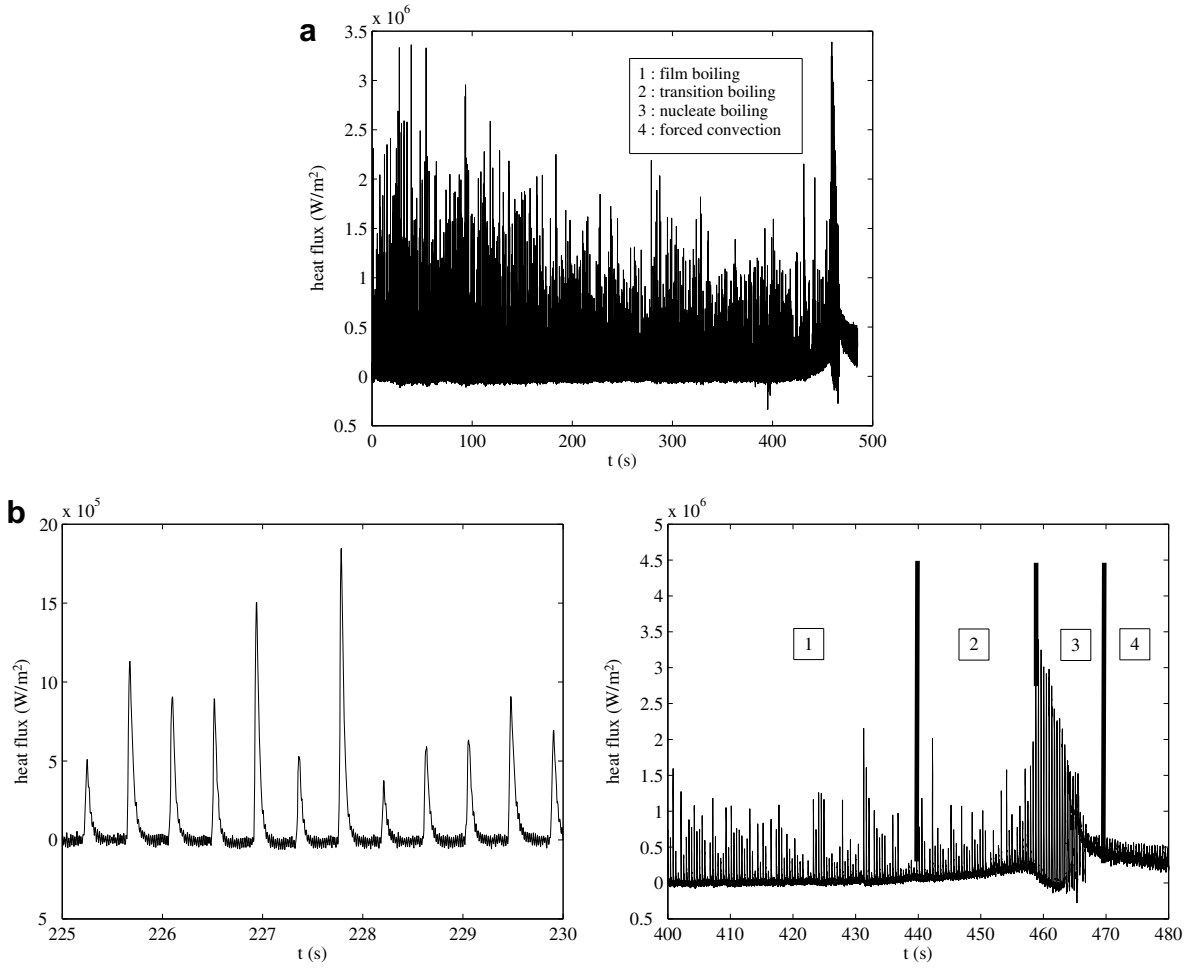

Fig. 15. Estimated heat flux in rotating case – $T_j = 66\ ^\circ C$, $r* = 1.25$ and $H = 50$ mm. (a) Estimated heat flux, (b) zoom of estimated heat flux in film boiling and end of cooling.

References

[1] J.-V. Beck, B. Blackwell, C.-R. St-Clair, Inverse Heat Conduction – Ill-Posed Problems, Wiley, New York, 1985.

[2] E.N. Wang, L. Zhang, L. Jiang, J.M. Koo, J. Maveety, E. Sanchez, K.E. Goodson, T.W. Kenny, Micromachined jets for liquid impingement cooling of VLSI chips, J. Microelectromech. Syst. 13 (2004) 833–842.

[3] X. Li, Study of the jet-flow rate of cooling in machining, Part 1. Theoretical analysis, J. Mat. Proc. Tech. 62 (1996) 149–156.

[4] X. Li, Study of the jet-flow rate of cooling in machining, Part 2. Simulation analysis, J. Mat. Proc. Tech. 62 (1996) 157–165.

[5] J. Hammad, Y. Mitsutake, M. Monde, Movement of maximum heat flux and wetting front during quenching of hot cylindrical block, Int. J. Therm. Sci. 43 (2004) 743–752.

[6] C.H. Huang, M.N. Ozisik, B. Sawaf, Conjugate gradient method for determining unknown contact conductance during metal casting, Int. J. Heat Mass Transfer 35 (1992) 1779–1786.

[7] C.H. Huang, T.M. Ju, A.A. Tseng, The estimation of surface thermal behavior of working roll in hot rolling process, Int. J. Heat Mass Transfer 38 (1995) 1019–1031.

[8] D.E. Hall, F.P. Incropera, R. Viskanta, Jet impingement boiling from a circular free-surface jet during quenching: part 1 – single-phase jet, J. Heat Transfer 123 (2001) 901–910.

[9] S. Peneau, J.P. Humeau, Y. Jarny, Front motion and convective heat flux determination in a phase change process, Inverse Problem Eng. 4 (1996) 53–91.

[10] F. Volle, D. Maillet, M. Gradeck, M. Lebouché, Semi-analytical inverse heat conduction on a rotating cylinder with Laplace and Fourier transforms, Inverse Problems Sci. Eng. 16 (2008) 655–674.

[11] D. Maillet, F. Volle, M. Gradeck, M. Lebouché, Estimation by an inverse method of boiling fluxes extracted by a water jet impinging on a hot rotating cylinder, Proceedings of the 13th International Heat Transfer Conference, Sydney, August 18–23, 2006, article BOI15, %3chttp://dx.doi.org/%3e doi:10.1615/IHTC13.p28.150, Begell House editor, 12 p., 2006.

[12] M. Gradeck, A. Kouachi, F. Volle, J.-L. Boréan, P. Gardin, M. Lebouché, Cooling of a hot cylinder with an impinging water jet, Proceedings of the 13th International Heat Transfer Conference, Sydney, August 18–23, 2006, article Jet-11, %3chttp://dx.doi.org/%3e) doi:10.1615/IHTC13.p16.100, Begell House editor, 12 p., 2006.

[13] H. Stehfest, Algorithm 368: numerical inversion of Laplace transforms, Commun. ACM 13 (1970) 47–49.

[14] H. Stehfest, Remark on algorithm 368: numerical inversion of Laplace transforms, Commun. ACM 13 (1970) 624.

[15] J.-V. Beck, K.J. Arnold, Parameter Estimation in Engineering and Science, Wiley, New York, 1977.

[16] A. Tikhonov, V. Arsenine, Méthodes de résolution des problèmes mal posés, Editions de Moscou, 1976.

[17] F. Volle, Conduction inverse sur un cylindre en rotation – Cas de l'ébullition convective induite par l'impact d'un jet d'eau, thèse de doctorat, Nancy-University, Nancy, France, 2006.

[18] A. Kouachi, Etude expérimentale de l'ébullition convective d'un jet d'eau plan impactant une surface mobile portée à hautes températures, thèse de doctorat, Nancy-University, Nancy, France, 2006.